Nanoscale Research Letters

NANO EXPRESS Open Access

Dichroic Optical Diode Transmission in Two Dislocated Parallel Metallic Gratings

Pengwei Xu[1], Xuefeng Lv[1], Jing Chen[1,2*], Yudong Li[1,2], Jun Qian[1], Zongqiang Chen[1], Jiwei Qi[1,2], Qian Sun[1,2,3*] and Jingjun Xu[1,2]

Abstract

An optical diode structure with two dislocated parallel metallic gratings is proposed and investigated numerically. Dichroic optical diode transmission is realized in this structure, i.e., optical diode effect is observed in two wavebands corresponding to inverse transmission directions. In the structure, two parallel metallic gratings with different grating constants are separated by a dielectric slab in between. The first illuminated grating acts as a selector for exciting surface plasmons at a proper wavelength. The other grating acts as an emitter to realize optical transmission. When the incident direction is reversed, the roles of two gratings exchange and surface plasmons are excited at another wavelength. In dichroic transmission wavebands, the optical diode structure exhibits extraordinary transmission and possesses high optical isolation up to 1. Furthermore, the operating wavebands can be modulated by changing structure parameters.

Keywords: Dichroic optical diode, Metallic gratings, Diffraction, Surface plasmons

Introduction

Optical diode, which transmits photons toward one direction and forbids the transmission in the reverse direction, has attracted considerable attention by virtue of the unidirectional transmission property [1]. Optical diode phenomena can be observed when time-reversal symmetry of light-matter interaction is broken. External magnetic field [2], bias voltage [3], acoustic wave [4], or time-dependent modulation [5, 6] can be applied to achieve the optical diode effect. In addition, the structure of spatial inversion symmetry breaking is an alternative choice, such as asymmetric multilayer structures [7], asymmetric photonic crystals [8], and asymmetric gratings [9]. In recent decades, metallic micro-nano structures gained great interest due to the promising properties of surface plasmons (SPs). Plasmonic devices are proposed in many research fields such as metasurface holography [10–14], refractive index sensor [15, 16], and filter [17, 18]. Plasmonic devices can strongly modify the interaction of electromagnetic fields in nanoscale [19]. The modulation on SPs can be realized through changing the surrounding dielectric environment and geometric parameters of metallic structures [20, 21]. Optical diodes composed of nanoscale metallic structures, for example, plasmonic layer sandwiched gratings [22, 23], cascaded plasmonic gratings [24, 25], plasmonic nanoholes [26], plasmonic slot waveguide [27], and plasmonic nanoparticle aggregates [28], are widely investigated for the purpose of optical information processing.

In this paper, dichroic optical diode transmission is obtained in two dislocated parallel metallic gratings sandwiching a dielectric slab. Both transmission enhancement and high isolation contrast ratio are achieved in the two operating wavebands with reverse transmission directions, because metallic gratings consisting of narrow slits exhibit extraordinary light transmission [29, 30] and asymmetric structures realize unidirectional transmission [27–31]. According to the illuminated order, two metallic gratings with different grating constants act as a selector and an emitter respectively. The selector selects the resonance wavelength by exciting SPs and, with the contribution of SPs, the emitter realizes light transmission. When the incident direction is reversed, the roles of two gratings exchange and SPs are excited at another wavelength. Therefore, the dichroic optical diode transmission is obtained. The thickness of the optical diode structure proposed in this paper is as

* Correspondence: jingchen@nankai.edu.cn; qiansun@nankai.edu.cn
[1]MOE Key Laboratory of Weak Light Nonlinear Photonics, Tianjin Key Laboratory of Photonics and Technology of Information Science, School of Physics, Nankai University, Tianjin 300071, China
Full list of author information is available at the end of the article

small as 160 nm. With the development of nanofabrication technologies, many methods can be applied to the fabrication of metallic gratings structures, such as ultraviolet nanoimprint lithography [32], laser-direct-writing lithography [33], and electron-beam lithography [34]. The optical diode character is independent of the incident intensity. These properties imply that our structure has extensive potentials in optical integration.

Methods

The scheme of optical diode structure is shown in Fig. 1. The structure consists of two silver gratings G_1 and G_2 sandwiching a silica layer. The thickness of silica layer is denoted as d. G_1 and G_2 have the same slit width s, the same thickness h, and different grating constants Λ_i ($i = 1, 2$). The structure is translational symmetric and the unit cell contains 2 units of G_1 and 3 units of G_2. Δ denotes the lateral relative position of G_1 and G_2 in a unit cell. Drude model [35] is used to describe the dielectric function of silver. The refractive index of silica is 1.5, ignoring its dispersion. The surrounding dielectric is air and its refractive index is 1. Normal incident plane wave of p-polarization is employed to investigate the optical diode effect.

Transmittance T of the optical diode structure is defined as follows:

$$T = \frac{p_o}{p_i}, \tag{1}$$

where P_i is the incident power and P_o is the output power. T is simulated numerically by using finite-difference time-domain (FDTD) method [36]. Periodic boundary conditions are employed to the left and right sides, and perfect matching layer boundaries are applied to the top and bottom sides of our simulation model. T_D and T_U represent the transmittance for downward incidence and upward incidence, respectively. The optical diode property is described by isolation contrast ratio η:

$$\eta = \frac{|T_D\text{-}T_U|}{T_D + T_U}. \tag{2}$$

Hence, $\eta = 1$ means the best optical diode performance.

Results and Theoretical Analyses

The transmittance and isolation contrast ratio of the optical diode structure are shown in Fig. 2. T_D is different to T_U when the incident wavelength is smaller than λ_C. T_D reaches the maximum value 0.73 and T_U is 3.7×10^{-3} at λ_D (1315 nm). Whereas T_U reaches the maximum value 0.82 and T_D is 3.6×10^{-4} at λ_U (921 nm). The isolation contrast ratios at λ_D and λ_U are 0.990 and 0.999, respectively. Figure 2 shows that optical diode effect is obtained at around λ_D and λ_U, and the two wavebands have reverse transmission directions. In the dichroic diode operating wavebands, the structure exhibits extraordinary transmission.

In order to understand the dichroic optical diode transmission, the electric field intensity $|E|^2$ at two operating wavebands are simulated. As shown in Fig. 3a, d, electric field is enhanced between two gratings when light transmits through the optical diode structure. Meanwhile, Fig. 3b, c show the reverse blocking status. The enhancement of electromagnetic field between two gratings is due to the SPs at two adjacent silver/silica interfaces. The types of SPs at two gratings are different, which are classified as structured SPs (SSPs) and induced SPs (ISPs) respectively. SSPs is excited and generates at the first illuminated grating (selector). ISPs is induced at the latter grating (emitter) by the coupling between SPPs and the adjacent silver/silica interface. Due to SSPs and ISPs, light transmits through the optical diode structure.

Surface charge density on the silver/silica interface and E_y component of the electric field distribution are illustrated in Fig. 4 to reveal the SPs coupling functions. In

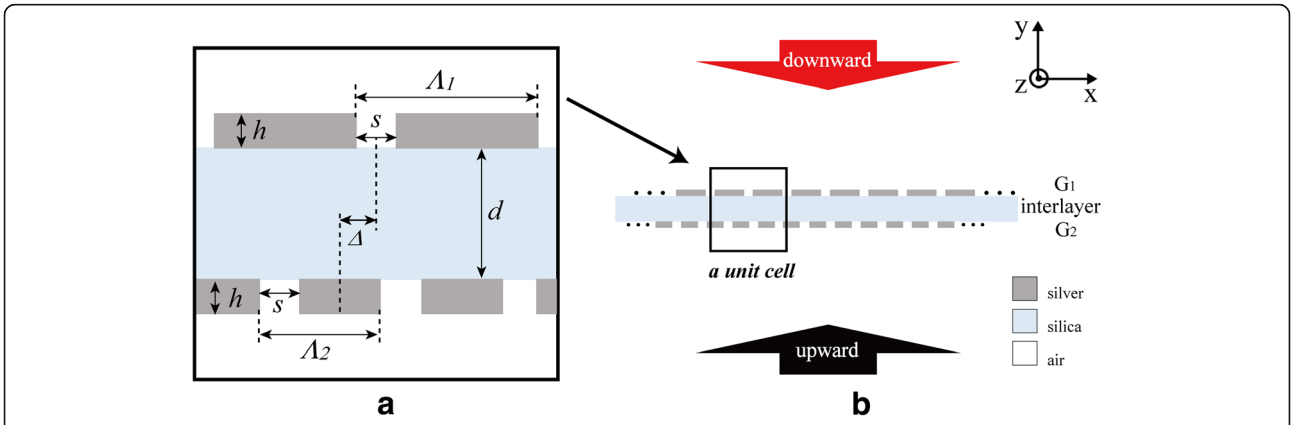

Fig. 1 Schematic diagram of optical diode structure. **a** The unit cell. **b** Overall view

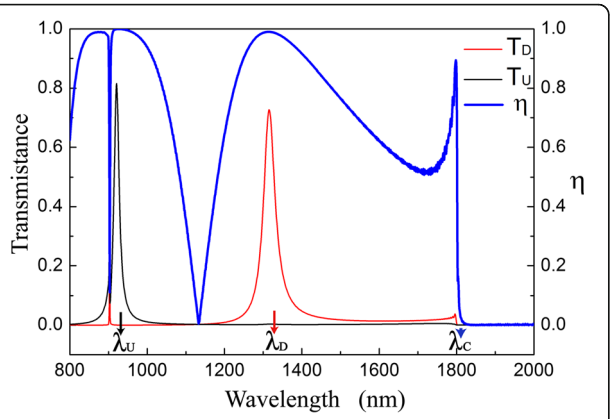

Fig. 2 Transmission spectra and the isolation contrast ratio of the optical diode structure with $d = 200$ nm, $s = h = 50$ nm, $\Lambda_1 = 900$ nm, $\Lambda_2 = 600$ nm, and $\Delta = 0$ nm

Fig. 4a, G_1 and G_2 have opposite charges on their adjacent surfaces, which is similar to flat plate capacitor. Under the condition of downward incidence, G_1 acts as a selector to excite SSPs at λ_D. The periodic surface charge density distribution represents that SPPs is determined by grating constant of G_1. G_2 supports the ISPs induced by SPPs and performs as an emitter for transmission. E_y between G_1 and G_2 is enhanced due to the coupling between SPPs and ISPs, as shown in Fig. 4b. For upward incident condition shown in Fig. 4c, d, G_2 acts as the selector and G_1 acts as the emitter.

As can be seen from Fig. 4, the transmission field is periodic and nonuniform in the horizontal (x-axis) direction. The period Λ ($\Lambda = 2\Lambda_1 = 3\Lambda_2$) of the transmission filed distribution is modulated by the integral optical diode structure and satisfies $2\pi/\Lambda = |g_1\text{-}g_2|$, here g_i is the grating vector of G_i ($i = 1, 2$). The grating diffraction efficiency is increased for the existence of SPs. The lateral wave vector κ of transmitted light derives from the superposition of g_1 and g_2:

$$\kappa = \pm\frac{2\pi}{\Lambda} = \pm|g_1 - g_2|, \tag{3}$$

And it decides the critical wavelength λ_C ($\lambda_C = 2\pi/|\kappa|$) for $T_D \neq T_U$. According to Eq. (3), λ_C is 1800 nm for our structure mentioned above, which is in good agreement with the simulation results $\lambda_C = 1806$ nm shown in Fig. 2. Optical diode effects appear in the range of $\lambda \leq \lambda_C$. According to the simulation results, the period of the integrated gratings (1800 nm) is larger than the diode operating wavelengths (1315 nm and 921 nm). Multi-order diffraction components can be obtained with light scattering from the integrated gratings. Thus, the transmission field is not uniform along the direction parallel to gratings, even when the light is transmitted to the far field.

SSPs of the silver grating are similar to SPs on planar silver/silica interface except that SSPs are radiative mode [37], while SPs are completely surface-bound modes. SSPs can be treated as SPs on planar silver/silica interface approximately when the slits of gratings are extremely narrow. So, the dispersion relation of SSPs can be written as [38] follows:

$$\beta = k_0\sqrt{\frac{\varepsilon_m\varepsilon_d}{\varepsilon_m + \varepsilon_d}} \tag{4}$$

where k_0 is the free space wave vector and ε_m and ε_d are the dielectric coefficient of silver and silica, respectively. The dispersion relation described by Eq. (4) is illustrated in Fig. 5. Dispersion curve calculated by using

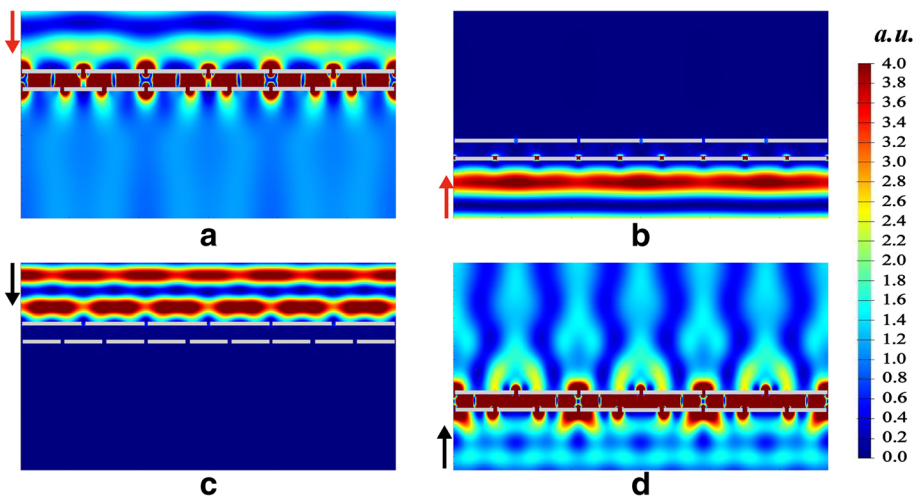

Fig. 3 Distributions of electric field intensity $|E|^2$ for downward incidence at $\lambda_D = 1315$ nm (**a**), upward incidence at $\lambda_D = 1315$ nm (**b**), downward incidence at $\lambda_U = 921$ nm (**c**), and upward incidence at $\lambda_U = 921$ nm (**d**)

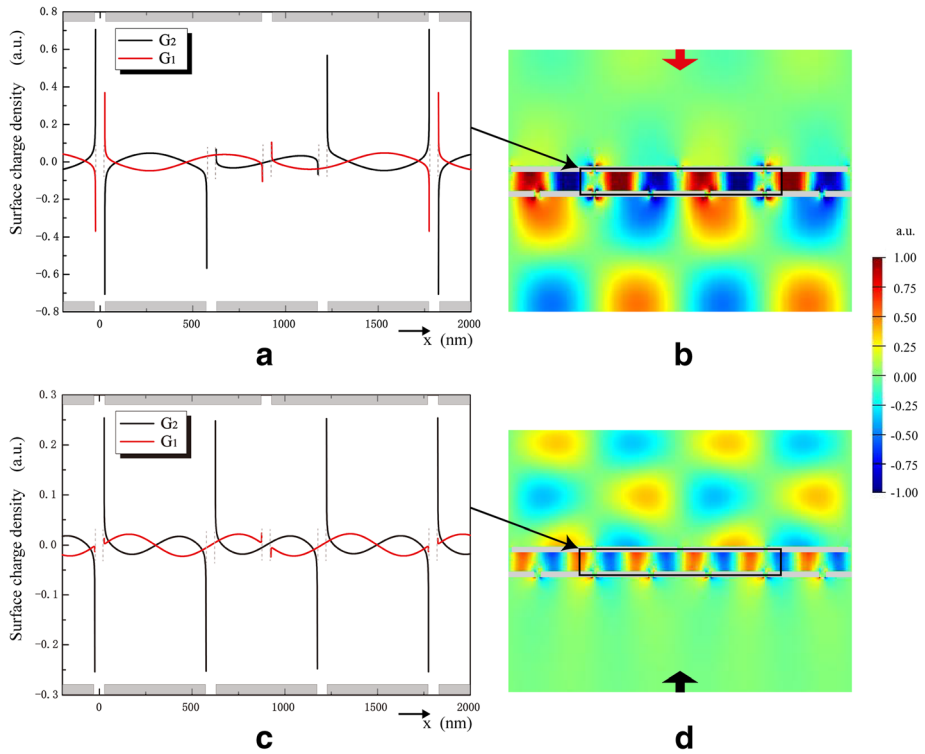

Fig. 4 The surface charge density on the silver/silica interface at G_1 and G_2, under the condition of downward incidence at $\lambda_D = 1315$ nm (**a**) and upward incidence at $\lambda_U = 921$ nm (**c**). *Ey* component of the electric field under the condition of downward incidence at $\lambda_D = 1315$ nm (**b**) and upward incidence at $\lambda_U = 921$ nm (**d**)

Drude model parameters [35] in this paper fits well with that calculated by using Johnson and Christy's optical constant data sets [39] when photon energy is below 2.75 eV ($\lambda > 450$ nm). In Fig. 5, the vertical red and black dash lines represent $|g_{1|}$ and $|g_2|$, respectively. SSPs is excited by the grating when the vector matching condition [40] is satisfied:

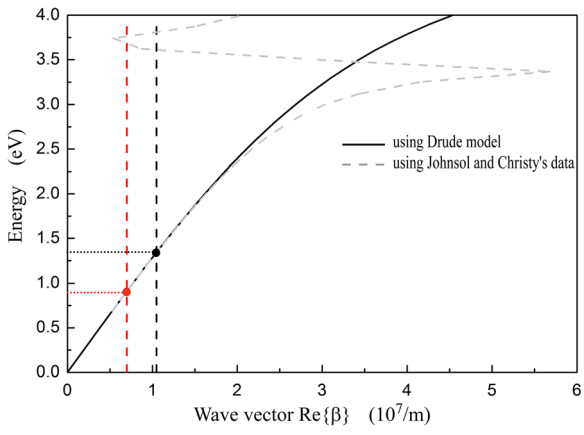

Fig. 5 Dispersion of SPs on planar silver/silica interface calculated by using Drude model and Johnson and Christy's optical constant data. The vertical red and black dash lines represent grating vector modulus $|g_1|$ and $|g_2|$, respectively

$$\beta = k_0 \sin\theta \pm N g_i (N = 1, 2, 3\ldots). \quad (5)$$

For normal incidence ($\theta = 0°$), the first-order ($N = 1$) diffraction of a grating has the highest diffraction efficiency, i.e., the largest excitation efficiency for SSPs. Thus, Eq. (5) is fulfilled at the red and black points shown in Fig. 5:

$$\beta = | g_i | . \quad (6)$$

In the optical diode structure, G_1 is the selector to excite SSPs for downward incidence and G_2 is the selector for upward incidence. G_1 and G_2 have different grating constants, so SSPs are excited at different wavelengths for reverse incident directions. In Fig. 5, the photon energy at the red point is 0.91 eV and the wavelength is 1365 nm, which is corresponding to λ_D (1315 nm) shown in Fig. 2. Similarly, the photon energy indicated by the black point is 1.04 eV and its wavelength is 924 nm, corresponding to λ_U (921 nm) in Fig. 2. As the approximation of grating to plate, the SSPs resonance wavelengths calculated by using Eq. (4) and Eq. (6) are not exactly equal to the ones simulated by using FDTD methods shown in Fig. 2.

Equation (5) indicates that incident angle θ influences the wave vector matching condition of grating to SSPs.

With the changing of θ, the transmittance and isolation contrast ratio at λ_D (1315 nm) and λ_U (921 nm) are simulated and shown in Fig. 6a, b, respectively. With θ increasing from 0° to 10°, T_D at λ_D and T_U at λ_U decrease for the wave vector mismatching between g_i and SSPs. (T_D at λ_D decreases to 0 when $\theta \approx 40°$ and T_U at λ_U decreases to 0 when $\theta \approx 35°$.) In incident angle range of $0° \le \theta \le 5°$, T_D at λ_U and T_U at λ_D are almost 0, and η always keeps larger than 0.98 at both λ_U and λ_D. Figure 6 demonstrates that the structure displays good optical diode effect at λ_D and λ_U under small-angle incidence.

Investigation and Discussion

In this section, we investigate the influence of structure parameters on transmission spectra and isolation contrast ratio.

The interlayer thickness d and gratings lateral relative position Δ are limited by fabrication accuracy. The influence of d and Δ on transmission spectra and the isolation contrast ratios are shown in Figs. 7 and 8, respectively. Figure 7 shows that the operating wavebands of optical diode exhibit a slight redshift when d increases. Meanwhile, the maximum value of T_D decreases very little, but the maximum value of T_U decreases significantly. The increase of d will lengthen the light transmission distance through the structure, weaken the electromagnetic interaction between G_1 and G_2, and impair the charge density induced at the surface of emitter. As seen in Fig. 4, charges distributed at slit corners of emitter act as electric dipoles sources of the transmission field. Charge density at slit corners of the emitter G_2 (Fig. 4a) is much greater than that at slit corners of the emitter G_1 (Fig. 4c), so d influences less on the maximum value of T_D than that of T_U. Besides, with the increase of d, small peaks marked as FP_1 and FP_2 appear in T_U and the transmission peak of FP_1 exhibits a large redshift. Electric filed intensity $|E|^2$ distributions prove that FP_1 and FP_2 result from Fabry-Perot resonances.

As shown in Fig. 1, the optical diode structure is periodic and it has the same unit cell when $\Delta = a \pm M\Lambda_2/2$ ($0 \text{ nm} < a < \Lambda_2/2$ and $M = 0, 1, 2\ldots$). Besides, the unit cell of $\Delta = a$ is left-right flip symmetric with that of $\Delta = -a \pm M\Lambda_2/2$ and they can realize the same transmission effect. So, the transmittance of the optical diode structure is affected by Δ as: $T(\Delta) = T(\Delta + \Lambda_2/2) = T(-\Delta + \Lambda_2/2)$. As shown in Fig. 8, optical diode effect at λ~921 nm turns on and off within a period of $\Lambda_2/2$ as Δ increases. However, transmission peak of T_D exhibits a slight blueshift and the optical diode effect at λ~1315 nm is always on when Δ increases. Seen in Fig. 8a, a new transmission peak at λ_N emerges in T_U curve near λ_U. When Δ increases from $\Lambda_2/12$ to $\Lambda_2/6$, the peak at λ_N exhibits a blueshift while the peak at λ_U exhibits a redshift (Fig. 8a, b). E_y distributions for transmission resonances at λ_U and λ_N are inserted in Fig. 8b. According to the simulation results, the resonance at λ_N generates because of the energy splitting. When Δ increases to $\Lambda_2/4$, shown in Fig. 8c, T_U is suppressed and two transmission resonances disappear, which makes the optical diode effect turn off at λ~921 nm.

According to the theory analysis, the operating waveband of optical diode can be obtained in a certain range by optimizing grating parameters. Figure 9 shows that the dichroic optical diode transmission is achieved in visible light range with structure parameters $d = 100$ nm, $\Lambda_1 = 450$ nm, $\Lambda_2 = 300$ nm, $s = h = 30$ nm, and $\Delta = 0$ nm. The maximum transmittances of dichroic diode transmission wavebands are 80% (at 522 nm for upward incidence) and 71% (at 732 nm for downward incidence), and the corresponding isolation contrast ratios η are 0.998 and 0.993.

Furthermore, the component of the unit cell in our structure also influences the optical diode phenomena. According to Eq. (5), the wavebands of diode effect depend on Λ_1 and Λ_2. In our research, we select the unit cell consisting of 2 units of G_1 and 3 units of G_2, i.e., $2\Lambda_1 = 3\Lambda_2$, in order to get high transmittances and good isolation contrast ratios in the optical diode wavebands simultaneously. For example, Fig. 10 shows the dichroic transmission of the optical diode structure with its unit cell consisting of 3 units of G_1 and 4 units of G_2. The optical diode effects are obtain at 530 nm with $T_U = 72\%$

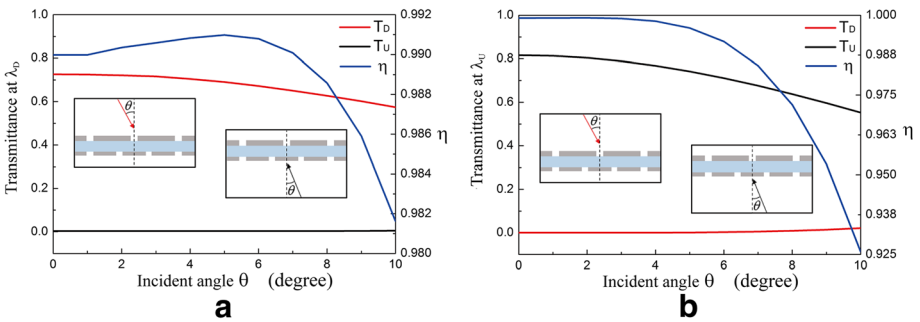

Fig. 6 The influence of incident angle on transmittance and isolation contrast ratio at $\lambda_D = 1315$ nm (**a**) and $\lambda_U = 921$ nm (**b**)

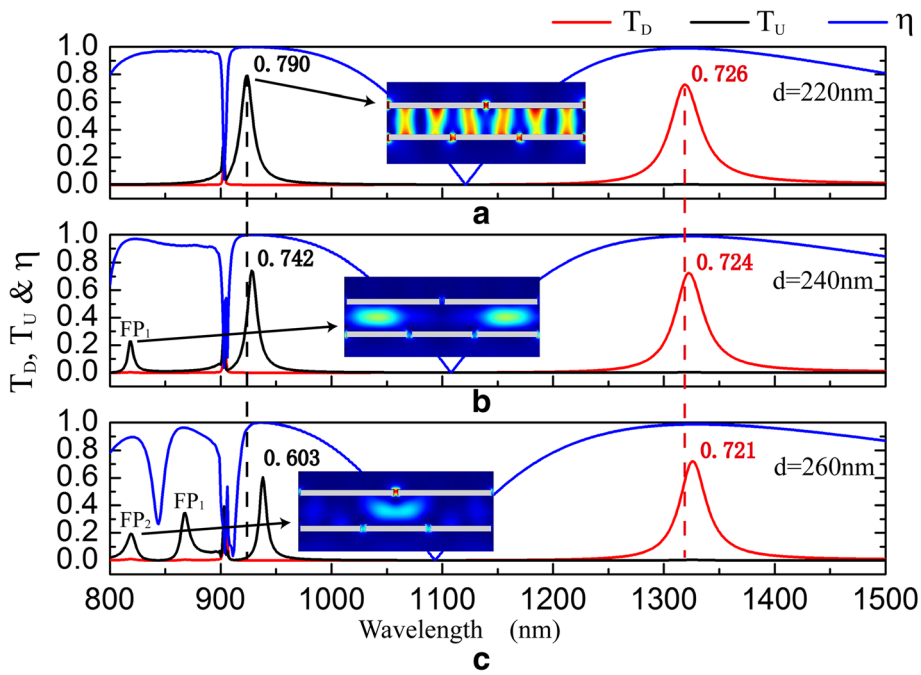

Fig. 7 The influence of d on transmission spectra and the isolation contrast ratio. $d = 220$ nm (**a**), $d = 240$ nm (**b**), and $d = 260$ nm (**c**) when $s = h = 50$ nm, $\Lambda_1 = 900$ nm, $\Lambda_2 = 600$ nm, and $\Delta = 0$ nm. The insets are distributions of electric field intensity $|E|^2$ for upward transmission resonances

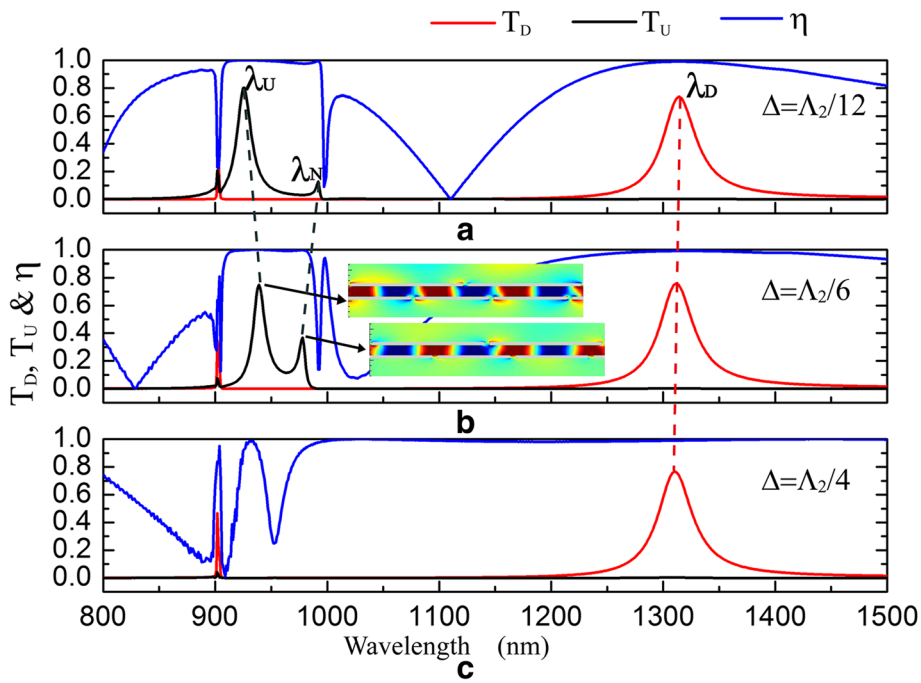

Fig. 8 The influence of Δ on transmission spectra and the isolation contrast ratio. $\Delta = 50$ nm $= \Lambda_2/12$ (**a**), $\Delta = 100$ nm $= \Lambda_2/6$ (**b**), and $\Delta = 150$ nm $= \Lambda_2/4$ (**c**) when $d = 200$ nm, $s = h = 50$ nm, $\Lambda_1 = 900$ nm, and $\Lambda_2 = 600$ nm. The insets in (**b**) are E_y distributions for upward transmission resonances

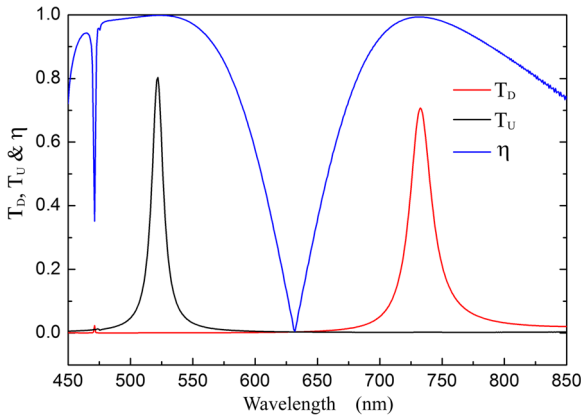

Fig. 9 Transmission spectra and isolation contrast ratio for the optical diode structure with $d = 100$ nm, $\Lambda_1 = 450$ nm, $\Lambda_2 = 300$ nm, $s = h = 30$ nm, and $\Delta = 0$ nm

and 659 nm with $T_U = 76\%$. The isolation contrast ratios at the two wavelengths are reduced to 0.912 and 0.987, because the difference of $|g_1|$ and $|g_2|$ is small and the grating acting as a selector can excite the SSPs of both gratings at different efficiencies. In addition, when $\Lambda_1 = 2\Lambda_2$, the SPs transmission resonance in the optical diode structure caused by the first-order diffraction of G_2 can also be excited by the second-order diffraction of G_1 for $2g_1 = g_2$, which would reduce the isolation contrast ratio. So, the good optical diode property requires that two grating constants should have a sufficient difference and avoid the integer multiple relationship.

Conclusions

The dichroic optical diode transmission based on SPs is realized in our structure, which consists of two dislocated parallel silver gratings and a silica interlayer. The first illuminated metallic grating selects the transmission waveband by exciting SSPs, and the other metallic grating emits electromagnetic energy forward through the surficial electrons oscillations. When the incident direction of light is reversed, the roles of two gratings exchange and another optical diode transmission waveband appears. The optical isolation ratio can almost reach up to 1. Optical diode transmission wavebands can be adjusted to be in different regions by changing the structure parameters. The optical diode operating wavebands and transmittance are independent of the incident intensity. The thickness of the structure is only a few hundred nanometers. These properties of our structure provide a wide range of applications in integrated circuits.

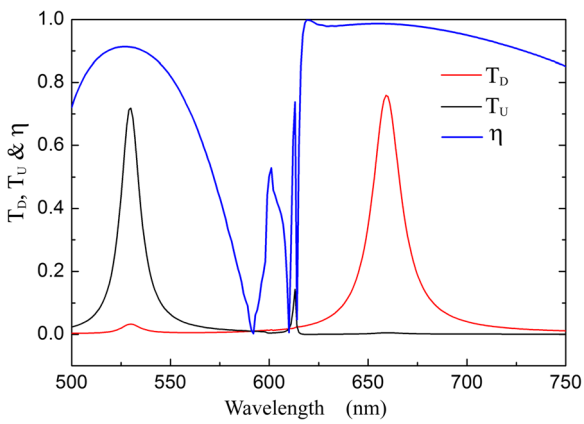

Fig. 10 Transmission spectra and the isolation contrast ratio for the optical diode structure with the unit cell including 3 units of G_1 and 4 units of G_2. $d = 100$ nm, $\Lambda_1 = 400$ nm, $\Lambda_2 = 300$ nm, $s = h = 30$ nm, and $\Delta = 0$ nm

Abbreviations

ISPs: Induced surface plasmons.; SPs: Surface plasmons; SSPs: Structured surface plasmons

Acknowledgements

Not applicable.

Funding

National Natural Science Foundation of China (11504185, 61178004, 11874229); Fundamental Research Funds for the Central Universities; Natural Science Foundation of Tianjin City (06TXTJJC13500); Science and Technology Commission of Tianjin Binhai New Area (BHXQKJXM-PT-ZJSHJ-2017003).

Availability of Data and Materials

The datasets supporting the conclusions of this article are included within the article.

Authors' Contributions

PX, QS, and JC initiated the idea. JQ provided FDTD Solutions for simulation and provided technical help. PX built the basic model and performed the simulations. PX, XL, JC, and QS participated in the analyses and discussion. PX and JC prepared the manuscript. All authors contributed to the revision of the manuscript. All authors read and approved the final manuscript.

Competing Interests

The authors declare that they have no competing interests.

Publisher's Note

Author details

[1]MOE Key Laboratory of Weak Light Nonlinear Photonics, Tianjin Key Laboratory of Photonics and Technology of Information Science, School of Physics, Nankai University, Tianjin 300071, China. [2]Collaborative Innovation Center of Extreme Optics, Shanxi University, Taiyuan 030006, Shanxi, China. [3]College of Environmental Science and Engineering/Sino-Canada R&D Center on Water and Environmental Safety, Nankai University, Tianjin 300071, China.

Received: 9 October 2018 Accepted: 23 November 2018
Published online: 04 December 2018

References

1. Fan L, Wang J, Varghese LT, Shen H, Niu B, Xuan Y, Weiner AM, Qi MH (2012) An all-silicon passive optical diode. Science. https://doi.org/10.1126/science.1214383
2. Shoji Y, Mizumoto T, Yokoi H, Hsieh IW (2008) Magneto-optical isolator with silicon waveguides fabricated by direct bonding. Appl Phys Lett. https://doi.org/10.1063/1.2884855

3. Song MH, Park B, Takanishi Y, Ishikawa K, Nishimura S, Toyooka T, Takezoe H (2006) Simple electro-tunable optical diode using photonic and anisotropic liquid crystal films. Thin Solid Films. https://doi.org/10.1016/j.tsf.2005.09.010
4. Wang Q, Xu F, Yu ZY, Qian XS, Hu XK, Lu YQ, Wang HT (2010) A bidirectional tunable optical diode based on periodically poled LiNbO3. Opt Express. https://doi.org/10.1364/OE.18.007340
5. Sounas DL, Alù A (2017) Non-reciprocal photonics based on time modulation. Nat Photonics. https://doi.org/10.1038/s41566-017-0051-x
6. Wang DW, Zhou HT, Guo MJ, Zhang JX, Evers J, Zhu SY (2013) Optical diode made from a moving photonic crystal. Phys Rev Lett. https://doi.org/10.1103/PhysRevLett.110.093901
7. Zhukovsky SV, Smirnov AG (2011) All-optical diode action in asymmetric nonlinear photonic multilayers with perfect transmission resonances. Phys Rev A. https://doi.org/10.1103/PhysRevA.83.023818
8. Serebryannikov AE, Cakmak AO, Ozbay E (2012) Multichannel optical diode with unidirectional diffraction relevant total transmission. Opt Express 20: 14980–14990
9. Li H, Deng Z, Huang J, Fu S, Li Y (2015) Slow-light all-optical soliton diode based on tailored Bragg-grating structure. Opt Lett 40:2572–2575
10. Deng Z-L, Deng J, Zhuang X et al (2018) Facile metagrating holograms with broadband and extreme angle tolerance. Light-Sci Appl 7:78
11. Deng Z-L, Deng J, Zhuang X et al (2018) Diatomic Metasurface for Vectorial holography. Nano Lett 18:2885–2892
12. Deng Z-L, Li G (2017) Metasurface optical holography. Mater Today Phys 3:16–32
13. Deng Z-L, Zhang S, Wang GP (2016) Wide-angled off-axis achromatic metasurfaces for visible light. Opt Express 24:23118–23128
14. Deng Z-L, Zhang S, Wang GP (2016) A facile grating approach towards broadband, wide-angle and high-efficiency holographic metasurfaces. Nanoscale 8:1588–1594
15. Wu D, Li R, Liu Y et al (2017) Ultra-narrow band perfect absorber and its application as Plasmonic sensor in the visible region. Nanoscale Res Lett 12:427
16. Chen C, Wang G, Zhang Z, Zhang K (2018) Dual narrow-band absorber based on metal–insulator–metal configuration for refractive index sensing. Opt Lett 43:3630–3633
17. Liang Y, Peng W, Lu M, Chu S (2015) Narrow-band wavelength tunable filter based on asymmetric double layer metallic grating. Opt Express 23:14434–14445
18. Kim H, Kim M, Chang T et al (2018) Bright and vivid plasmonic color filters having dual resonance modes with proper orthogonality. Opt Express 26: 27403–27417
19. Davoyan AR, Engheta N (2013) Nonreciprocal rotating power flow within plasmonic nanostructures. Phys Rev Lett. https://doi.org/10.1103/PhysRevLett.111.047401
20. Hohenau A, Leitner A, Aussenegg FR (2007) Near-field and far-field properties of nanoparticle arrays. In: Brongersma ML, Kik PG (eds) Surface plasmon nanophotonics. Springer, Dordrecht, pp 11–25
21. Chen Z-x, Chen J-h, Wu Z-j, Hu W, Zhang X-j, Lu Y-q (2014) Tunable Fano resonance in hybrid graphene-metal gratings. Appl Phys Lett. https://doi.org/10.1063/1.4873541
22. Serebryannikov A, Ozbay E (2009) Isolation and one-way effects in diffraction on dielectric gratings with plasmonic inserts. Opt Express. https://doi.org/10.1364/OE.17.000278
23. Serebryannikov A, Ozbay E (2009) Unidirectional transmission in non-symmetric gratings containing metallic layers. Opt Express. https://doi.org/10.1364/OE.17.013335
24. Zhu Z, Liu K, Xu W, Luo Z, Guo C, Yang B, Ma T, Yuan X, Ye W (2012) One-way transmission of linearly polarized light in plasmonic subwavelength metallic grating cascaded with dielectric grating. Opt Lett. https://doi.org/10.1364/OL.37.004008
25. Xu J, Cheng C, Kang M, Chen J, Zheng Z, Fan YX, Wang HT (2011) Unidirectional optical transmission in dual-metal gratings in the absence of anisotropic and nonlinear materials. Opt Lett 36:1905–1907
26. Peng N, She W (2014) Asymmetric optical transmission through periodic arrays of cone air holes in a metal film. Opt Express. https://doi.org/10.1364/OE.22.028452
27. Hu XY, Zhang YB, Xu XA, Gong QH (2011) Nanoscale surface plasmon all-optical diode based on plasmonic slot waveguides. Plasmonics. https://doi.org/10.1007/s11468-011-9243-2
28. Brullot W, Swusten T, Verbiest T (2015) Broadband nonreciprocal quadrupolarization-induced asymmetric transmission (Q-AT) in plasmonic nanoparticle aggregates. Adv Mater. https://doi.org/10.1002/adma.201405409
29. Barbara A, Quemerais P, Bustarret E, Lopez-Rios T (2002) Optical transmission through subwavelength metallic gratings. Phys Rev B. https://doi.org/10.1103/PhysRevB.66.161403
30. Deng Z, Cao Y, Li X, Wang G (2018) Multifunctional metasurface: from extraordinary optical transmission to extraordinary optical diffraction in a single structure. Photonics Res 6:443–450
31. Zhang Y, Kan Q, Wang GP (2014) One-way optical transmission in silicon grating-photonic crystal structures. Opt Lett 39:4934–4937
32. Hwang J, Oh B, Kim Y et al (2018) Fabry-Perot cavity resonance enabling highly polarization-sensitive double-layer gold grating. Sci Rep 8:14787
33. Ali R, Saleem MR, Roussey M et al (2018) Fabrication of buried nanostructures by atomic layer deposition. Sci Rep 8:15098
34. Liu X, Gao J, Gao J et al (2018) Microcavity electrodynamics of hybrid surface plasmon polariton modes in highquality multilayer trench gratings. Light-Sci. Appl. 7:14
35. Xu P, Zhang M, Chen Z, Qi J, Chen J, Qian J, Li Y, Sun Q, Xu J (2018) Unidirectional optical transmission in a single-layer metallic grating consisting of cambered resonantors. IEEE Photonics J. https://doi.org/10.1109/JPHOT.2018.2850321
36. Taflove A, Hagness SC (2005) Computational electrodynamics: the finite-difference time-domain method, 3rd edn. Artech House, Boston
37. Huang XR, Peng RW (2010) General mechanism involved in subwavelength optics of conducting microstructures: charge-oscillation-induced light emission and interference. J Opt Soc Am A. https://doi.org/10.1364/JOSAA.27.000718
38. Karpinski P, Miniewicz A (2011) Surface plasmon polariton excitation in metallic layer via surface relief gratings in photoactive polymer studied by the finite-difference time-domain method. Plasmonics. https://doi.org/10.1007/s11468-011-9234-3
39. Johnson PB, Christy RW (1972) Optical constants of the noble metals. Phys Rev B 6:4370–4379
40. Koev ST, Agrawal A, Lezec HJ, Aksyuk VA (2012) An efficient large-area grating coupler for surface Plasmon Polaritons. Plasmonics. https://doi.org/10.1007/s11468-011-9303-7